Experimental Validation of Stable Coordination for Multi-Robot Systems with Limited Fields of View using a Portable Multi-Robot Testbed

Pratik Mukherjee[1], Matteo Santilli[2], Andrea Gasparri[2] and Ryan K. Williams[1]

***Abstract*— In this paper, we address the problem of stable coordinated motion in multi-robot systems with limited fields of view (FOVs). These problems arise naturally for multi-robot systems that interact based on sensing, such as our case study of multiple unmanned aerial vehicles (UAVs) each equipped with several cameras that are used for detecting neighboring UAVs. In this context, our contributions are: i) first, we derive a framework for studying stable motion and distributed topology control for multi-robot systems with limited FOVs; and ii) Then, we provide experimental results in indoor and challenging outdoor environments (e.g., with wind speeds up to 10 mph) with a team of UAVs to demonstrate the performance of the proposed control framework using a portable multi-robot experimental set-up.**

I. Introduction

Multi-robot systems are experiencing a surge in interest from the robotics community. With the success of single robot systems over the past decade, the promise of meaningful multi-robot applications beyond laboratory environments has steadily increased. In particular, the rapid advancement in perception, embedded computation, point-to-point communication, and the availability of reliable and robust off-the-shelf robotic platforms have been key to recent success in the area of multi-robot systems. Indeed, multi-robot systems are being actively deployed in various important applications, including search and rescue missions [1], autonomous inventory management [2], and precision agriculture [3]. However, there are important theoretical and application oriented issues unique to multi-robot systems which must be overcome. In this paper, our concern will be *interaction* in distributed multi-robot systems with perception that is limited in its field of view (FOV).

When operating in a distributed setting where global information is not available to all robots, a multi-robot system must rely on perceptual sensors like cameras, laser range finders, ultrasonic detectors, etc., that exhibit limited fields of view. From a theoretical perspective, limited field-of-view perception induces *asymmetry* in robot-to-robot interaction which introduces the possibility of degeneracies in typical coordinated motion control schemes [4]–[12]. In fact, our recent work [13] has demonstrated that unlike symmetrically interacting systems, asymmetric interactions must be carefully chosen to yield stable and safe coordinated motion.

[1]P. Mukherjee and R.K. Williams are with Electrical and Computer Engineering Department, Virginia Polytechnic Institute and State University, Blacksburg, VA USA, {mukhe027, rywilli1}@vt.edu

[2]M. Santilli and A. Gasparri are with the Engineering Department, Roma Tre University Roma, 00146, Italy, matteo.santilli@uniroma3.it, gasparri@dia.uniroma3.it

Related work can be separated into three topics: asymmetric motion control, interaction optimization, and applications of perception in multi-robot systems. Work in asymmetric motion control is relatively new, with recent examples like [14], where the authors address the edge agreement problem of second-order non-linear multi-agent systems under quantized measurements for directed graphs. More generally, various prior works such as [15] have accounted for multi-agent systems over directed networks, often with the *assumption* that the graph is strongly connected. Topology control for directed graphs is also quite sparse, with recent examples [13], [16], [17] focusing on overcoming the theoretical shortcuts that are lost when the symmetry assumption is broken. Interaction optimization is instead a more mature area, with examples including connectivity maximization [18], [19] and optimal rigid graph construction for multi-agent localization [20]. Finally, several recent works have exploited advanced perception in multi-robot systems, with examples including [21] which achieves multi-target tracking with camera-equipped unmanned aerial vehicles (UAVs), [22] which applies collaborative structure from motion for UAV formation control and [23] which demonstrates a distributed optimization framework for multi-robot collaborative tasks using vision. [24] has also demonstrated the use of a multi-robot system for various multi-robot collaborative applications in different experimental settings using onboard sensors.

While recent work has made progress in each of the three areas outlined, we propose in this work a problem that spans asymmetric control and realistic multi-robot perception. We further validate the theoretical findings using a *portable multi-robot experimental setup* based on ultra-wide band localization. This portable testbed gives us the capability to validate our methods with the logical progression of testing our work first in simulation, then in controlled indoor environments and finally in realistic outdoor environments. In this regard, our contribution is twofold. First, we extend our framework [13] to study stable motion and distributed topology control for multi-robot systems with limited FOVs. Then, we provide experimental results with a team of DJI Matrice 100 UAVs performing motion control with limited FOVs to demonstrate the proposed control framework.

II. Preliminaries

Consider a multi-robot system composed of n robots, each having motion that evolves according to the following

dynamics

$$\dot{x}_i(t) = u_i(t) \tag{1}$$

with $x_i(t) \in \mathbb{R}^d$ the robot state (position), $u_i(t) \in \mathbb{R}^d$ the control input, and time $t \in \mathbb{R}_{\geq 0}$. Stacking robot states and inputs yields the overall system

$$\dot{\mathbf{x}}(t) = \mathbf{u}(t) \tag{2}$$

with $\mathbf{x}(t) = [x_1^T(t), \ldots, x_n^T(t)]^T \in \mathbb{R}^{nd}$ and $\mathbf{u}(t) = [u_1^T(t), \ldots, u_n^T(t)]^T \in \mathbb{R}^{nd}$ the stacked vector of states and control inputs, respectively. The distance between robots i and j is denoted by $\|x_{ij}(t)\| \triangleq \|x_i(t) - x_j(t)\|$, with the standard Euclidean norm. Note that dependence on time, state, and/or a graph will only be shown when introducing new concepts or symbols. Subsequent usage will drop these dependencies for clarity of presentation.

We assume the robots possess proximity-limited communication and sensing with limited field of view, yielding robot-to-robot interactions that change over time according to system motion. Let us model the robot-to-robot (communication and sensing) interactions by means of a dynamic directed graph denoted by $\mathcal{G}(t) \triangleq (\mathcal{V}, \mathcal{E}(t))$ with node set $\mathcal{V} \triangleq [v_1, ..., v_n]$ and edge set $\mathcal{E}(t) \subseteq \mathcal{V} \times \mathcal{V}$. Regarding proximity-limited communication, let us define radii $\rho_{i,c} \in \mathbb{R}_+, \forall\, i \in \{1, \ldots, n\}$, within which communication can occur for each robot. As a result, we can define the communication graph $\mathcal{G}_c = (\mathcal{V}, \mathcal{E}_c)$ with edges $\mathcal{E}_c = \{(i,j) \,|\, \|x_{ij}\| \leq \rho_{i,c}, i, j \in \mathcal{V}\}$. Regarding sensing with limited field of view, let us define for each robot i the set of functions $S_i = \left\{s_i^k \triangleq s(x_i, \theta_i^k, \alpha_i^k, \rho_{i,s}^k),\ k = 1, \ldots, m_i\right\}$ encoding the m_i circular (or spherical) sectors where α_i^k denotes the central angle of the k-th circular sector located at x_i of radius $\rho_{i,s}^k$ and of orientation θ_i^k. As a result, we can define the sensing graph as $\mathcal{G}_s = (\mathcal{V}, \mathcal{E}_s)$ with edges $\mathcal{E}_s = \{(i,j) \,|\, x_j \in S_i, i, j \in \mathcal{V}\}$. Later, we will also introduce $\mathcal{G}_s^{\text{FOV}} = \{\mathcal{V}, \mathcal{E}_s^{\text{FOV}}\}$ the interaction graph encoding pairwise sensing interactions with limited field of view which is the same as $\mathcal{G}_s$ except sensing with limited FOV. This four field-of-view sensing model is motivated by the UAV platform we currently use for experiments. The reader is referred to Figure 1 for a graphical representation of a robot possessing proximity-limited communication and sensing with limited FOVs.

In the case of directed graphs, the edge (i,j) indicates *asymmetric* interaction (sensing or communication) between a robot i and another robot j. Denote by $\mathcal{N}_i^+(t) := \{j \in \mathcal{V} : (i,j) \in \mathcal{E}(t)\}$ the set of *out-neighbors* of robot i and $\mathcal{N}_i^-(t) := \{j \in \mathcal{V} : (j,i) \in \mathcal{E}(t)\}$ the set of *in-neighbors*. In the sequel, we will always refer by $\mathcal{N}_i^+$ and $\mathcal{N}_i^-$ to the *sensing* out-neighborhood and in-neighborhood, respectively. It is also assumed that $(i,i) \notin \mathcal{E}$. In addition, when referencing single edges we will use two conventions: e_k is the k-th directed edge out of $|\mathcal{E}|$ total edges, whereas e_{ij} is the directed edge leaving from vertex v_i and entering vertex v_j.

The *incidence matrix* $\mathcal{B}(\mathcal{G}(t)) \in \mathbb{R}^{n \times |\mathcal{E}|}$ of a graph $\mathcal{G}$, is a matrix with rows indexed by robots and columns indexed by edges, such that $\mathcal{B}_{ij} = 1$ if the edge e_j leaves vertex v_i, -1 if it enters vertex v_i, and 0 otherwise. The *outgoing incidence matrix* $\mathcal{B}_+$ contains only the outgoing parts of the incidence matrix $\mathcal{B}$, with incoming parts set to zero. The *undirected Laplacian matrix* $\mathcal{L} \in \mathbb{R}^{n \times n}$ is obtained as $\mathcal{L} = \mathcal{B}\mathcal{B}^T$, whereas the *directed Laplacian matrix* $\mathcal{L}_d \in \mathbb{R}^{n \times n}$ is computed as $\mathcal{L}_d = \mathcal{B}\mathcal{B}_+^T$. The undirected Laplacian matrix $\mathcal{L}$ is symmetric positive-semidefinite, whereas the directed Laplacian matrix $\mathcal{L}_d$ is generally asymmetric and indefinite. We will also make use of the *undirected edge Laplacian* $\mathcal{L}_\mathcal{E} \in \mathbb{R}^{|\mathcal{E}| \times |\mathcal{E}|}$ defined as $\mathcal{L}_\mathcal{E} = \mathcal{B}^T\mathcal{B}$ and the *directed edge Laplacian* $\mathcal{L}_\mathcal{E}^d \in \mathbb{R}^{|\mathcal{E}| \times |\mathcal{E}|}$ given by $\mathcal{L}_\mathcal{E}^d = \mathcal{B}^T\mathcal{B}_+$. For properties of the edge Laplacian see for example [25] and [14].

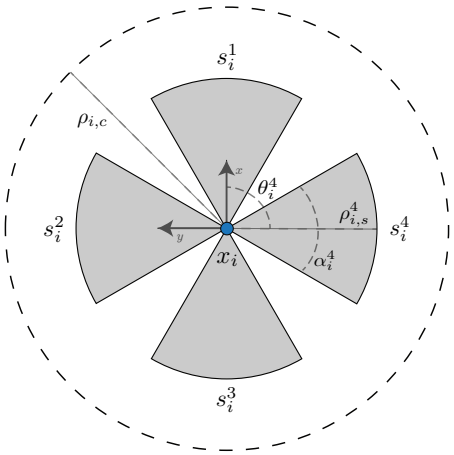

Fig. 1. Modeling of proximity-limited communication with radius $\rho_{i,c}$ and sensing with limited fields of view $S_i = \{s_i^1, s_i^2, s_i^3, s_i^4\}$ for a robot i

III. Stable Directed Coordination with FOVs

A. Directed Coordination Framework

Potential-based control design is a commonly used framework for controlling multi-robot systems [4]–[12]. The basic idea is to encode the energy of a system as a potential function $V(\mathbf{x}(t)) \in \mathbb{R}_+$ such that the desired configurations of the multi-robot system correspond to critical points. Thus, a control law can be designed to achieve these configurations by driving the system along the negative-gradient $\mathbf{u} = -\nabla_\mathbf{x} V$. Control objectives that are pairwise, and thus distributed across a multi-robot system, can be designed by associating a (continuously differentiable[1]) potential function $V_{ij}(\mathbf{x}) \triangleq V_{ij}(x_i, x_j) \in \mathbb{R}_+$ with robots i and j. The control input for the i-th robot is then defined as

$$u_i(t) = -\sum_{j \in \mathcal{N}_i^+} \nabla_{x_i} V_{ij} = -\sum_{j \in \mathcal{N}_i^+} a_{ij}(\|x_{ij}(t)\|) x_{ij} \tag{3}$$

where $a_{ij}(\|x_{ij}(t)\|) \in \mathbb{R}$ is a smooth, time-varying scalar weight function that can take arbitrary values for edges $(i,j) \in \mathcal{E}$, and where a_{ij} does not necessarily equal a_{ji}.

Now, let the Lyapunov function $V : \mathbb{R}^{nd} \to \mathbb{R}_+$ be a continuously differentiable function, defined in the standard

[1] A generalization to handle non-smooth potential functions can be found in [11], [26]. Here, for the sake of simplicity, smooth pairwise potentials are assumed.

manner

$$V(\mathbf{x}(t)) = \sum_{i=1}^{n} \sum_{j \neq i} V_{ij}(\|x_{ij}\|) \tag{4}$$

with time derivative

$$\dot{V} = (\nabla_{\mathbf{x}} V)^T \, \dot{\mathbf{x}} \tag{5}$$

from simple application of the chain rule. As detailed in [13], it is possible to derive a convenient *edge-based* form of $\nabla_{\mathbf{x}} V$ and $\dot{\mathbf{x}}$ that will eventually reveal the graph topology and (5) can be rewritten as

$$\dot{V} = -\xi^T \left[\mathcal{L}_{\mathcal{E}}^d \otimes I_d \right] \xi = -\mathbf{x}^T \left[\left(\mathcal{B} W \mathcal{L}_{\mathcal{E}}^d W \mathcal{B}^T \right) \otimes I_d \right] \mathbf{x} \tag{6}$$

where from [13], we have a weighted version of ξ defined as

$$\xi = \left(W(t) \mathcal{B}^T \otimes I_d \right) \mathbf{x} \tag{7}$$

with $W(t) = \operatorname{diag}\left(\left[a_{e_1}, \ldots, a_{e_{|\mathcal{E}|}} \right] \right)$ where it can be noticed that further topological structure is given to the variable ξ. With the addition of the time-varying weight matrix W, proving stability means that it is necessary to prove that for *every* matrix W encoding a certain potential-based control at any time t, the asymmetric matrix $\mathcal{B} W \mathcal{L}_{\mathcal{E}}^d W \mathcal{B}^T \in \mathbb{R}^{n \times n}$ is positive semidefinite. Instead, we want to know for *any* weight matrix W if the system is stable. This question is captured by the following result from [13] with a correction.

Lemma 1. *For any* $W = \operatorname{diag}\left(\left[a_{e_1}, \ldots, a_{e_{|\mathcal{E}|}} \right] \right) \in \mathbb{R}^{|\mathcal{E}| \times |\mathcal{E}|}$ *associated with* $\mathcal{G}_s$*, there exists* $\widehat{W}$ *such that*

$$\left(W \mathcal{B}^T \otimes I_d \right) = \left(\mathcal{B}^T \widehat{W} \otimes I_d \right) \tag{8}$$

whenever $\mathcal{B}^T \mathcal{B} \triangleq \mathcal{L}_{\mathcal{E}}$ *is invertible.*

Next, by applying Lemma 1 to (6), we obtain

$$\dot{V} = -\xi^T \left[\left(\mathcal{B}^T \mathcal{B}_+ \right) \otimes I_d \right] \xi = -\mathbf{z}^T \left[\underbrace{\left(\mathcal{L} \mathcal{L}_d^T \right)}_{S} \otimes I_d \right] \mathbf{z} \tag{9}$$

with $\mathbf{z} = (\widehat{W} \otimes I_d)\mathbf{x} \in \mathbb{R}^{nd}$ and $S \in \mathbb{R}^{n \times n}$ the *structural Lypaunov matrix*, where by structural we refer to the fact that this matrix is by construction compatible with the network sensing graph $\mathcal{G}_s$ and independent of the system state between changes in $\mathcal{G}_s$.

We can now notice that the Lyapunov time derivative in (9) is in a typical quadratic form and the characteristics of this quadratic equation are dependent on the properties of the *structural Lyapunov matrix* S. However, as the S matrix is asymmetric in nature, the typical algebraic definition of positive semi-definiteness does not apply (i.e., non-negativity of eigenvalues). Hence, the Lyapunov stability analysis is carried out on the symmetrized S, $S^+ = \frac{1}{2}(S + S^T)$, as positive semi-definiteness of S^+ implies positive semi-definiteness of S. The following theorem from [13] provides a sufficient condition for establishing the stability of directed potential-based objectives.

Theorem 1. *Assuming the conditions for Lemma 1 hold, and* $1/2[(\mathcal{B}^T \mathcal{B}_+) + (\mathcal{B}_+)^T (\mathcal{B})]$ *is positive definite, the system* (1) *with robot controls* (3) *is stable in the sense that if* V *is initially finite it remains finite for all time* $t > 0$*.*

B. Coordination Framework with Limited Field of View

So far, a stable motion framework for multi-robot systems with directed interactions has been reviewed and for more clarity we refer the reader to [13]. Notably, the underlying assumption of this framework is that each robot has its own proximity-limited communication and sensing capability described by two radii $\rho_{i,c}, \rho_{i,s} \in \mathbb{R}_+, \forall i \in \{1, \ldots, n\}$, within which sensing and communication can occur for each robot, respectively. We are now interested in taking a step further and deriving a mathematical modeling for sensing with limited fields of view. From the previous section it follows that our objective can be stated as the problem of finding a way of modeling pairwise directed interactions based on sensing with limited fields of view, by means of a composition of pairwise gradients satisfying the requirements outlined above.

In order to proceed, first we need to provide a mathematical formalization of pairwise directed interactions with limited field of view. In this regard, let us denote with $\mathcal{G}_s^{\text{FOV}} = \{\mathcal{V}, \mathcal{E}_s^{\text{FOV}}\}$ the interaction graph encoding pairwise sensing interactions with limited field of view. At this point, let us introduce an extended state $\mathbf{x_i}$ defined as

$$\mathbf{x_i} = \Big[x_i^{\circ T}, x_i^{\triangleleft,1 T}, x_i^{\triangledown,1 T}, x_i^{\triangleright,1 T}, \ \ldots \\ \ldots, \ x_i^{\triangleleft,m_i T}, x_i^{\triangledown,m_i T}, x_i^{\triangleright,m_i T} \Big]^T$$

for each robot composed of the robot location itself, that is $x_i^{\circ} = x_i$, and a set of virtual points $\{x_i^{\triangleleft,k}, x_i^{\triangledown,k}, x_i^{\triangleright,k}\}$ that move as if they were rigidly attached to a robot i for each circular sector k belonging to the limited field of view S_i. Note that, the position of each set of virtual points $\{x_i^{\triangleleft,k}, x_i^{\triangledown,k}, x_i^{\triangleright,k}\}$ is defined according to the orientation θ_i^k of the k-th circular sector to which such set is associated, that is $x_i^{\tau,k} = R_i^{\tau,k}(x_i)\, x_i + t_i^{\tau,k}(x_i)$ where $\{R_i^{\tau,k}(x_i), t_i^{\tau,k}(x_i)\}$ are pairs of proper rotation matrices and translation vectors and τ is an element of the set $\mathcal{T} \triangleq \{\triangleleft, \triangledown, \triangleright\}$ denoting the virtual points.

At this point, for each robot i we can introduce an approximation $\tilde{s}_i^k$ of the k-th circular (or spherical) sector s_i^k as

$$\tilde{s}_i^k = \left\{ x \in \mathbb{R}^d : \|x_i^{\circ} - x\| \leq \rho_{i,1}^k \ \wedge \ \|x_i^{\tau,k} - x\| \geq \rho_{i,2}^k \right\} \tag{10}$$

for all $\tau \in \mathcal{T}$ and $\rho_{i,1}^k, \rho_{i,2}^k \in \mathbb{R}_+$ two radii chosen in such a way to approximate the k-th circular (or spherical) sector of the i-th robot as defined by $s(x_i, \theta_i^k, \alpha_i^k, \rho_{i,s}^k)$, where $\wedge$ is the logical "and" operator. Therefore, it follows that given two robots i and j with state x_i and x_j respectively, we say that the robot j is within the limited sensing field of view of robot i if there exists at least one approximation[2] $\tilde{s}_i^k$ with $k \in \{1, \ldots, m_i\}$, such that $x_j \in \tilde{s}_i^k$. The reader is referred to Figure 2 for a graphical representation of the set of logical conditions given in (10).

[2]If there is more than one circular (spherical) sector for which $x_j \in \tilde{s}_i^k$ then we assume robot i locally selects the best one according to some sensing metric. This guarantees that our sensing graph does not become a multigraph.

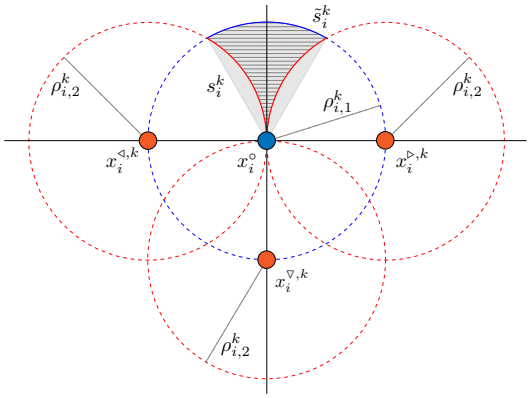

Fig. 2. Approximation $\tilde{s}_i^k$ of the k-th circular sector s_i^k for the limited field of view S_i of an robot i by means of the set of logical conditions given in (10).

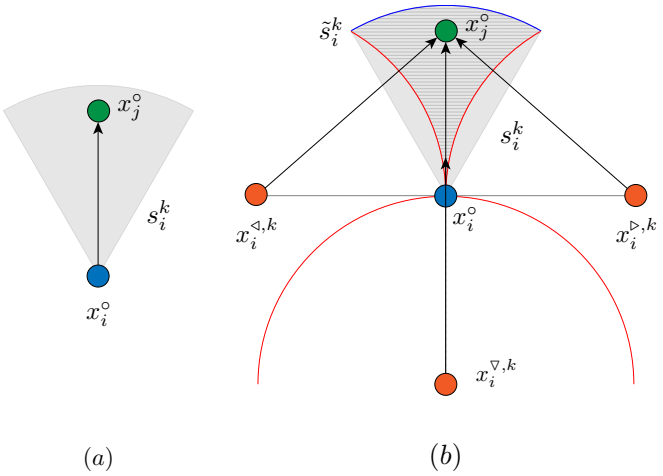

Fig. 3. Mapping between the interaction graph $\mathcal{G}_s^{\text{FOV}} = \{\mathcal{V}, \mathcal{E}_s^{\text{FOV}}\}$ encoding the pairwise interactions with limited field of view and the interaction graph $\overline{\mathcal{G}}_s^{\text{FOV}} = \{\overline{\mathcal{V}}^{\text{FOV}}, \overline{\mathcal{E}}_s^{\text{FOV}}\}$ encoding the equivalent pairwise interactions with limited field of view for the extended system modeling.

We are now ready to illustrate how by introducing for each robot i the extended state $\mathbf{x_i}$, it is possible to approximate any desired pairwise sensing interaction with limited field of view. Intuitively, the idea is that for each edge $(i,j) \in \mathcal{G}_s^{\text{FOV}}$ we can use a set of virtual points $\{x_i^{\triangleleft,k}, x_i^{\triangledown,k}, x_i^{\triangleright,k}\}$ along with the actual robot location x_i° to describe the desired interaction by means of a proper combination of gradients satisfying the requirements previously outlined. This allows us to derive a modeling of the multi-robot system with limited field of view, which we will refer to as the *extended system*, which is amenable to the theoretical framework described above.

As a case study, let us consider the maintenance of a desired topological property $\mathbb{P}$ as the design objective for the pairwise directed sensing interaction with limited field. More specifically, to the scope of this paper, let us assume the topological property of interest to be the maintenance of a directed link $(i,j) \in \mathcal{E}$. Notably, this objective can be translated in a setting with limited field of view by considering the following extended dynamics of each robot i:

$$\dot{x}_i^\circ = \underbrace{-\sum_{j \in \mathcal{N}_i^+} \left(\nabla_{x_i^\circ} V_{ij}^\circ + \sum_{\tau \in \mathcal{T}} \nabla_{x_i^{\tau,k_j}} V_{ij}^{\tau,k_j} \right)}_{u_i} \tag{11}$$

with $\dot{x}_i^{\tau,q} = u_i, q = 1,\dots,m_i$ for each virtual point $\tau \in \mathcal{T}$, where $\mathcal{N}_i^+ = \{j \in \mathcal{V}, \,|\, (i,j) \in \mathcal{E}_s^{\text{FOV}}\}$ is defined according to (10), k_j denotes the index k for which $x_j \in \tilde{s}_i^k$ with $k = 1,\dots,m_i$ and the potentials $V_{ij}^\circ(\|x_i^\circ - x_j\|)$, $V_{ij}^{\tau,k_j}(\|x_i^\tau - x_j\|)$ can be chosen such that

$$\begin{aligned} V_{ij}^{\circ,k_j}(\|x_i^\circ - x_j\|) &\to \infty \quad \text{as } \|x_i^\circ - x_j\| \to \rho_{i,1}^k, \\ V_{ij}^{\tau,k_j}(\|x_i^\tau - x_j\|) &\to \infty \quad \text{as } \|x_i^\tau - x_j\| \to \rho_{i,2}^k. \end{aligned} \tag{12}$$

Interestingly, two things can be noticed from (11): i) the actual dynamics of the robot x_i° is influenced by the interactions of its m_i sets of virtual points $\{x_i^{\triangleleft,k}, x_i^{\triangledown,k}, x_i^{\triangleright,k}\}$, and ii) the dynamics of the m_i sets of virtual points $\{\dot{x}_i^{\triangleleft,k}, \dot{x}_i^{\triangledown,k}, \dot{x}_i^{\triangleright,k}\}$ are identical to the actual dynamics of the robot $\dot{x}_i^\circ$ being them rigidly attached to it.

At this point, it becomes clear that we can study the stability of a multi-robot system $\mathbf{x} = [x_1^T, \dots, x_n^T]^T$ with limited field of view, by checking the stability of its extended version $\overline{\mathbf{x}} = [\mathbf{x_1}^T, \dots, \mathbf{x_n}^T]^T$. To this end, starting from the interaction graph $\mathcal{G}_s^{\text{FOV}} = \{\mathcal{V}, \mathcal{E}_s^{\text{FOV}}\}$, which encodes the pairwise interactions with limited field of view, we require a systematic way for constructing the interaction graph $\overline{\mathcal{G}}_s^{\text{FOV}} = \{\overline{\mathcal{V}}^{\text{FOV}}, \overline{\mathcal{E}}_s^{\text{FOV}}\}$, which encodes the equivalent pairwise interactions with limited field of view for its modeling based on the extended system. Indeed, this will permit to build the incidence matrices $\overline{\mathcal{B}}$ and $\overline{\mathcal{B}}_+$ associated to the graph $\overline{\mathcal{G}}_s^{\text{FOV}}$ which are required to check the stability of the multi-robot system with limited field of view by inspecting its extended system as per Theorem 1.

At this point, in order to derive a systematic way to build the interaction graph $\overline{\mathcal{G}}_s^{\text{FOV}}$ it suffices to notice that: i) for each vertex $i \in \mathcal{V}_{\text{FOV}}$ of the system with limited field of view, the extended system has $3\,m_i + 1$ vertexes, that is $\{i^\circ, i^{\triangleleft,1}, i^{\triangledown,1}, i^{\triangleright,1}, \dots, i^{\triangleleft,m_i}, i^{\triangledown,m_i}, i^{\triangleright,m_i}\} \in \overline{\mathcal{V}}^{\text{FOV}}$; and ii) for each directed edge $(i,j) \in \mathcal{E}_s^{\text{FOV}}$ of the system with limited field of view, the extended system has four edges, that is $\{(i^\circ, j^\circ), (i^{\triangleleft}, j^\circ), (i^{\triangledown}, j^\circ), (i^{\triangleright}, j^\circ)\} \in \overline{\mathcal{E}}_s^{\text{FOV}}$. The reader is referred to Figure 3 for a graphical interpretation of this mapping. Notably, the well defined structure underlying this mapping also permits to easily identify a deterministic mapping between the two incidence matrices $\mathcal{B}$ and $\mathcal{B}_+$ of $\mathcal{G}_s^{\text{FOV}}$ and their counterparts $\overline{\mathcal{B}}$ and $\overline{\mathcal{B}}_+$ of $\overline{\mathcal{G}}_s^{\text{FOV}}$. Given such as mapping, we can directly verify the stability of coordinated topology control with limited FOVs through application of Theorem 1. Intuitively, the idea is to: i) consider an extended state with $4|\mathcal{E}_s|$ virtual points taken as replica of the actual agents; ii) perform a suitable algebraic manipulation of the extended state to zero out portions of the contributions corresponding to non-interacting virtual points and iii) finally apply Theorem 1 on the resulting extended states, yielding guaranteed stability. Since this paper focuses on experimental validation and for the sake of brevity, a rigorous proof of the application of Theorem 1 to verify stability is not included.

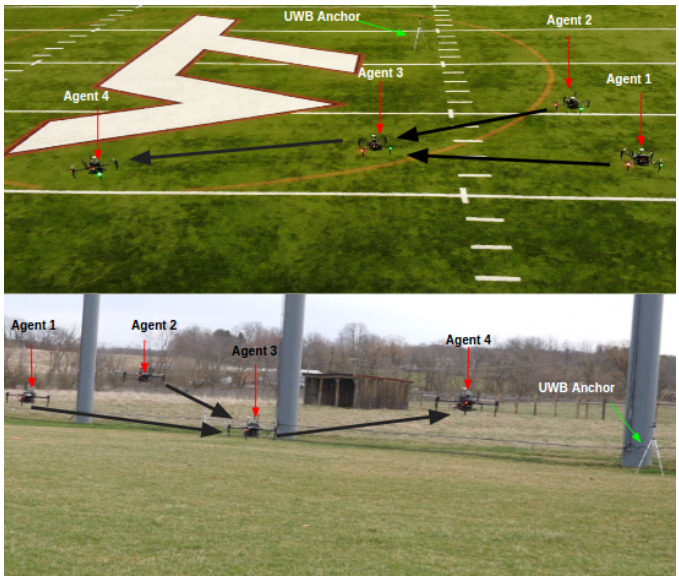

Fig. 4. Four DJI Matrice 100s forming and maintaining a preselected stable directed interaction graph in outdoor (bottom) and indoor(top) environments.

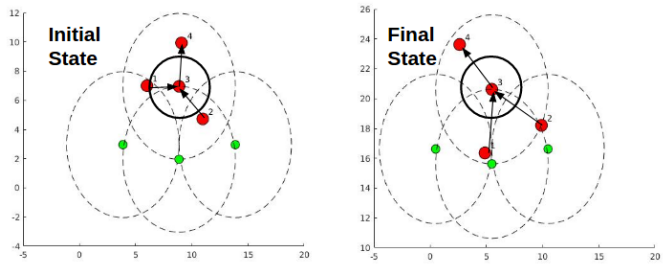

Fig. 5. Initial and final states of the all agents(red circles) in an indoor experiment with agent 4 in agent 3's FOV(one forward facing circular sector) represented by FOV radii of the three virtual points(green circles) of agent 3 and the collision radius represented by solid black circle around agent 3.

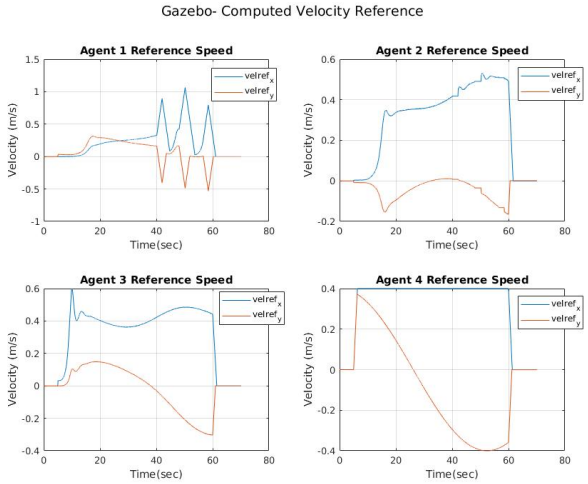

Fig. 6. Computed velocity reference from FOV controller for agents 1,2 and 3 in Gazebo with agent 4 receiving a predetermined velocity.

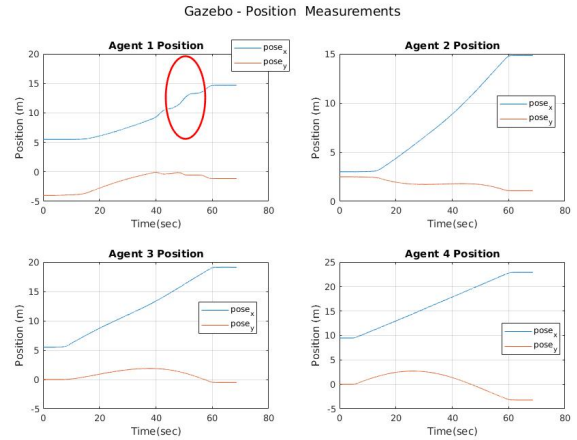

Fig. 7. Position measurement data for Gazebo simulation where agent 4 moves in oscillatory trajectory (y-position data) and all other agents act to keep their neighbors in their respective FOVs.

IV. Portable Multi-Robot Experimental Setup

We deployed a team of DJI Matrice 100 (M100) UAVs and used an ultra-wideband (UWB) system, Pozyx [27], for localization of the UAVs to control a stable FOV topology according to our theoretical results. To conduct experiments of topology control using onboard UWB localization, we place six Pozyx anchor UWB nodes in the environment as shown in Figure 4. Individual UWB tags are then mounted on each of the UAVs from which the position measurement is obtained. In the video of the experiment submitted, we demonstrate limited FOV topology control of four UAVs operating in an area of 30m $\times$ 20m. A stable directed interaction graph was preselected as represented in Figures 4 and 5 and this graph is maintained by all agents during experimentation. Also, note that the orientation of x and y axes used in Gazebo and actual experiments differ and hence there is a difference in orientation of measurements between Gazebo and experiments.

1) Gazebo Simulation Results: It is evident in Figure 7 that agent 4 (leader) tracks a predetermined velocity reference shown in Figure 6. To test the FOV controller's capability to tackle a non-trivial trajectory, we intentionally chose the velocity profile of the leader agent to have a cosine oscillation. Consequently, the FOV controller computes reference velocities for agents 3,2 and 1 such that they maintain their neighbors in their respective FOVs as shown for agent 3 in Figure 5. From simulations, we realized that the dynamics of the selected graph was such that agents 1 and 2 kept approaching each other very closely. Hence, collision avoidance is implemented which ensures all agents remain out of each other's collision radii[3] and still remain connected as shown in Figure 5. This is also evident in the oscillating trend in the x-axis position (region inside red circle) data in Figure 7 of agent 1 between 40 and 60 seconds where agent 1 moves in and out of agent 2's collision radius.

[3]Note that the collision radius in figure 5 is for diagrammatic representation only and does not accurately represent the actual size of the radius used for experiments.

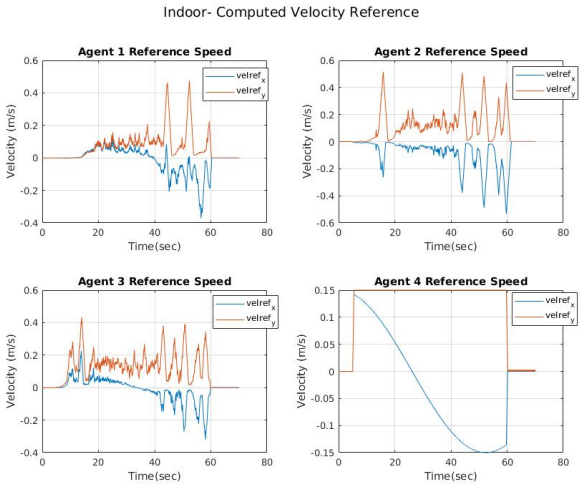

Fig. 8. Computed velocity reference from FOV controller for agents 1,2 and 3 from indoor experiment with agent 4 receiving a predetermined velocity.

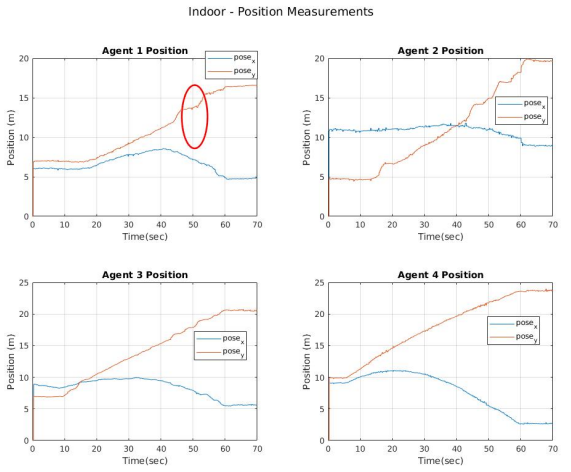

Fig. 9. Pozyx position measurement data for agents from indoor experiment.

2) Indoor Football Facility : The velocity reference profiles, Figure 8, differ for the M100s when compared to the UAV models in Gazebo due to the different underlying controllers of the two systems and their physical differences. However, the position data profiles, Figure 9, for all agents are similar to that obtained from Gazebo simulation. For instance, the position data of agents 1 and 2 in Figure 9 clearly show that both agents move in and out of their collision radius having the same oscillatory trend (in and around red circle of agent 1's y-position data) visible between 40 and 60 seconds and also the cosine oscillation trend is prominently visible in the x-position data of all agents, similar to leader agent 4.

3) Outdoor Drone Park : With wind speeds of approximately 10 mph, Figures 10 and 11 show the results of the outdoor experiment. The results are similar to that of the experiment conducted indoors. There is some induced noise from the environmental disturbance evident in the position measurement

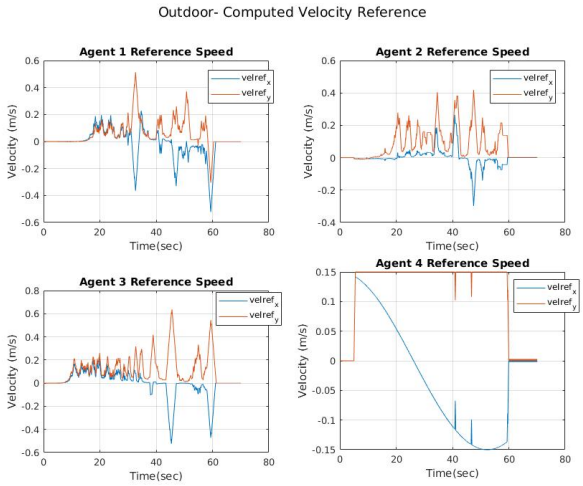

Fig. 10. Computed velocity reference from FOV controller for agents 1,2 and 3 from outdoor experiment with agent 4 receiving a predetermined velocity.

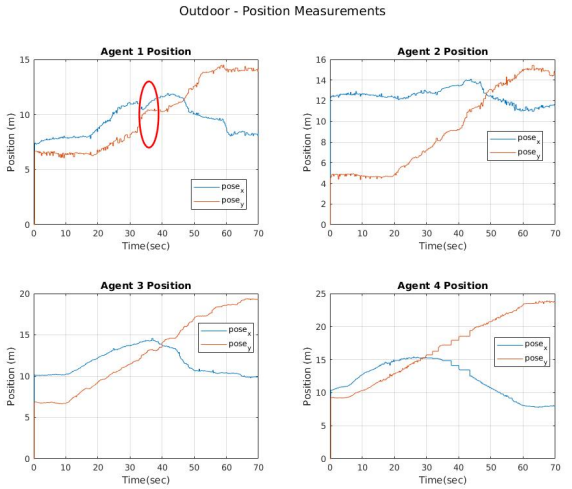

Fig. 11. Pozyx position measurement data for agents from outdoor experiment with induced noise from windy outdoor conditions.

data in Figure 11. However, the controller appears to behave similar to the indoor experiment, with agents 1 and 2 moving in and out of each other's collision radii (region in and around red circle in figure 11).

V. Conclusions

In this paper,we extended a framework we developed for studying stable motion and distributed topology control for multi-robot systems with directed interactions to the case of a multi-robot system with limited fields of view. Then, we provided experimental results with a team of DJI Matrice 100 UAVs that demonstrated the effectiveness of the control framework and showcased a *portable multi-robot experimental setup*.

REFERENCES

[1] G. Bevacqua, J. Cacace, A. Finzi, and V. Lippiello, "Mixed-initiative planning and execution for multiple drones in search and rescue missions." in *ICAPS*, 2015, pp. 315–323.

[2] E. Guizzo, "Three engineers, hundreds of robots, one warehouse," *IEEE spectrum*, vol. 45, no. 7, pp. 26–34, 2008.

[3] P. Tripicchio, M. Satler, G. Dabisias, E. Ruffaldi, and C. A. Avizzano, "Towards smart farming and sustainable agriculture with drones," in *Intelligent Environments (IE), 2015 International Conference on*. IEEE, 2015, pp. 140–143.

[4] D. E. Koditschek and E. Rimon, "Robot navigation functions on manifolds with boundary," *Advances in Applied Mathematics*, vol. 11, no. 4, pp. 412 – 442, 1990.

[5] M. M. Zavlanos and G. J. Pappas, "Potential fields for maintaining connectivity of mobile networks," *IEEE Transactions on Robotics*, vol. 23, no. 4, pp. 812–816, Aug 2007.

[6] M. Ji and M. Egerstedt, "Distributed coordination control of multiagent systems while preserving connectedness," *IEEE Transactions on Robotics*, vol. 23, no. 4, pp. 693–703, Aug 2007.

[7] D. V. Dimarogonas and K. J. Kyriakopoulos, "Connectedness preserving distributed swarm aggregation for multiple kinematic robots," *IEEE Transactions on Robotics*, vol. 24, no. 5, pp. 1213–1223, Oct 2008.

[8] M. M. Zavlanos, H. G. Tanner, A. Jadbabaie, and G. J. Pappas, "Hybrid control for connectivity preserving flocking," *IEEE Transactions on Automatic Control*, vol. 54, no. 12, pp. 2869–2875, Dec 2009.

[9] H. G. Tanner, A. Jadbabaie, and G. J. Pappas, "Flocking in fixed and switching networks," *IEEE Transactions on Automatic Control*, vol. 52, no. 5, pp. 863–868, May 2007.

[10] R. K. Williams and G. S. Sukhatme, "Constrained Interaction and Coordination in Proximity-Limited Multi-Agent Systems," *IEEE Transactions on Robotics*, vol. 29, pp. 930–944, 2013.

[11] R. K. Williams, A. Gasparri, G. S. Sukhatme, and G. Ulivi, "Global connectivity control for spatially interacting multi-robot systems with unicycle kinematics," in *2015 IEEE International Conference on Robotics and Automation (ICRA)*, May 2015, pp. 1255–1261.

[12] A. Gasparri, L. Sabattini, and G. Ulivi, "Bounded control law for global connectivity maintenance in cooperative multirobot systems," *IEEE Transactions on Robotics*, vol. 33, no. 3, pp. 700–717, June 2017.

[13] P. Mukherjee, A. Gasparri, and R. K. Williams, "Stable motion and distributed topology control for multi-agent systems with directed interactions," in *Decision and Control (CDC), 2017 IEEE 56th Annual Conference on*, 2017.

[14] Z. Zeng, X. Wang, and Z. Zheng, "Edge agreement of multi-agent system with quantised measurements via the directed edge laplacian," *IET Control Theory Applications*, vol. 10, no. 13, pp. 1583–1589, 2016.

[15] J. Mei, W. Ren, and J. Chen, "Distributed consensus of second-order multi-agent systems with heterogeneous unknown inertias and control gains under a directed graph," *IEEE Transactions on Automatic Control*, vol. 61, no. 8, pp. 2019–2034, 2016.

[16] M. M. Asadi, A. Ajorlou, and A. G. Aghdam, "Distributed control of a network of single integrators with limited angular fields of view," *Automatica*, vol. 63, pp. 187–197, 2016.

[17] L. Sabattini, C. Secchi, and N. Chopra, "Decentralized estimation and control for preserving the strong connectivity of directed graphs," *IEEE Trans Cybern*, vol. 45, no. 10, pp. 2273–2286, Oct. 2015.

[18] P. Yang, R. A. Freeman, G. J. Gordon, K. M. Lynch, S. S. Srinivasa, and R. Sukthankar, "Decentralized estimation and control of graph connectivity for mobile sensor networks," *Automatica*, vol. 46, no. 2, pp. 390–396, 2010.

[19] R. K. Williams and G. S. Sukhatme, "Locally constrained connectivity control in mobile robot networks," in *2013 IEEE International Conference on Robotics and Automation*, May 2013, pp. 901–906.

[20] A. Gasparri, R. K. Williams, A. Priolo, and G. S. Sukhatme, "Decentralized and Parallel Constructions for Optimally Rigid Graphs in R^2," *IEEE Transactions on Mobile Computing*, vol. 14, no. 11, pp. 2216–2228, Nov. 2015. [Online]. Available: http://ieeexplore.ieee.org/document/7018921/

[21] P. Tokekar, V. Isler, and A. Franchi, "Multi-target visual tracking with aerial robots," in *2014 IEEE/RSJ International Conference on Intelligent Robots and Systems*. IEEE, 2014, pp. 3067–3072.

[22] E. Montijano, E. Cristofalo, D. Zhou, M. Schwager, and C. Sagüés, "Vision-Based distributed formation control without an external positioning system," *IEEE Trans. Rob.*, vol. 32, no. 2, pp. 339–351, Apr. 2016.

[23] R. Tron, J. Thomas, G. Loianno, K. Daniilidis, and V. Kumar, "A distributed optimization framework for localization and formation control: Applications to vision-based measurements," *IEEE Control Systems Magazine*, vol. 36, no. 4, pp. 22–44, Aug 2016.

[24] M. Saska, T. Ba, J. Thomas, J. Chudoba, L. Preucil, T. Krajnk, J. Faigl, G. Loianno, and V. Kumar, "System for deployment of groups of unmanned micro aerial vehicles in gps-denied environments using onboard visual relative localization," *Autonomous Robots*, vol. 41, 04 2016.

[25] D. Zelazo, A. Rahmani, and M. Mesbahi, "Agreement via the edge laplacian," in *2007 46th IEEE Conference on Decision and Control*, Dec 2007, pp. 2309–2314.

[26] R. K. Williams, A. Gasparri, G. Ulivi, and G. S. Sukhatme, "Generalized topology control for nonholonomic teams with discontinuous interactions," *IEEE Transactions on Robotics*, vol. 33, no. 4, pp. 994–1001, Aug 2017.

[27] P. Dabove, V. D. Pietra, M. Piras, A. A. Jabbar, and S. A. Kazim, "Indoor positioning using ultra-wide band (uwb) technologies: Positioning accuracies and sensors' performances," in *2018 IEEE/ION Position, Location and Navigation Symposium (PLANS)*, April 2018, pp. 175–184.